CANCOM2024 – CANADIAN INTERNATIONAL CONFERENCE ON COMPOSITE MATERIALS

BIOINSPIRED MANDREL-BED 3D PRINTING ENHANCES DAMGE TOLERANCE OF NANOCOMPOSITE

Patil, Haresh[1], Mondal, Dibakar[1], Hashemi, Sanaz S.[1], and Willett, Thomas L.[1]*
1 Systems Design Engineering, University of Waterloo, Waterloo, Canada
* Corresponding author (thomas.willett@uwaterloo.ca)

Keywords*:* Nanocomposites, Direct Ink Writing, Mandrel, Interfaces

ABSTRACT

Biological materials such as wood, bone, bamboo are natural composites. They have developed remarkable damage tolerance through crack deflection at weak interfaces in their hierarchically organized, concentrically layered, lamellar microstructures. This work demonstrates a novel approach to mimic such concentric layer microstructure with mandrel-bed Direct Ink Writing (DIW) to print robust nanocomposite structures. Since photopolymerization exhibits stiffness transition at the interface bonding of 3D printed layers, a method of controlling damage tolerance of DIW printed structure by tuning interface bonding was also discussed.
Four photocurable nanocomposites were prepared by dispersing heat treated hydroxyapatite nano particles (nHA) into a functionalized biopolymer resins composed of: 1) Acrylated Epoxidized Soybean Oil (AESO) and polyethylene glycol diacrylate (PEGDA) as diluent, 2) methacrylate functionalized AESO (mAESO) and PEGDA, and third and fourth nanocomposite was prepared by replacing a small volume of PEGDA with tri glycerol diacrylate (TGDA) as a building block monomer in the resins described above. Concentrically layered Crisscross (+/-45°) microstructures were printed of all four nanocomposite inks and twisted ply (Bouligand) microstructures were printed using the third nanocomposite composition using the mandrel bed 3D printer. Single Edge Notched Beams (SENB) were cut from the printed microstructures. SENB specimens were also cast in a machined PTFE mold using all nanocomposite inks for isotropic control. The fracture toughness of all printed and cast SENB specimens was measured using fracture tests (based on ASTM-E1820) to evaluate the significance of the interfaces on damage tolerance/fracture resistance. Scanning electron microscopy (SEM) images of printed microstructures revealed distinct and differentiable interfaces in the mandrel bed printed microstructures. The 3D printed Crisscross microstructures had lower fracture toughness than the respective isotropic controls. Bouligand microstructures improved the fracture toughness over the isotropic control. The interfaces in the printed microstructures were more effective in enhancing damage tolerance of nanocomposite. This work provides valuable insights regarding interfaces developed in DIW printed photocurable nanocomposites structures and their effectiveness in tuning damage tolerance of the 3D printed structures.

1 INTRODUCTION

Composite materials may be used to produce mechanically competent parts with low weight to strength ratio if engineered with an appropriate composition of physical, structural and chemical characteristics of two or more materials. Studies of bioinspired composites have reported remarkable improvement in damage tolerance of unidirectional fiber composite structures [1], [2]. Natural materials such as wood, bone, etc. are natural composites [3], [4]. Wood is a polymeric composite and bone is a composite of organic-inorganic phases comprised of nano size inorganic mineral arranged in mostly collagen [3], [4]. The concentrically layered lamellar microstructure of

mineralized fibrils and weak interfaces in such microstructure are though to provide the extraordinary damage tolerance of natural materials [4], [5]. Nanocomposites have attracted researchers due to their ability to reduce defect size and to have a greater interaction with matrix through their high surface area to volume ratios [6].

Fabricating nanocomposite parts with conventional molding and layup methods is laborious. Nanocomposites containing photocurable thermoset resin mixed with an appropriate photoinitiator enables their 3D printing. Direct ink writing (DIW) is a cost-effective material extrusion-based method of 3D printing; it permits exceptional flexibility with material and processing condition of printing. DIW allows customized material deposition in a programmable pattern. Conventional flatbed DIW stacks planar material layers to fabricate parts. The photocurable nanocomposite activates free radical polymerization on exposure of appropriate UV intensity which crosslinks the functional groups to solidify the deposited feedstock (raster). Polymerization also bonds newly deposited raster to previously cured raster, which develops an interface. Previous masked stereolithography 3D printing studies have reported that change in crosslinking density at the interfaces reduced the stiffness of the material at the interfaces [7], [8]. Mimicking concentrically layered microstructure with 3D printing is a novel approach to fabricate robust structures with nanocomposites. Flatbed 3D printing inhibits mimicking concentrically layered lamellar microstructures of biomaterials. Mandrel bed DIW is a novel approach of printing parts with concentric layers on a rotating print bed mimicking the lamellar microstructure of wood and bone. DIW allows one to tune the mechanical properties of the printed parts by controlling microstructural anisotropy [9], [10]. However, the contribution of the interfaces to the mechanical properties of DIW printed structures remains unevaluated.

This work demonstrates a novel approach to tune damage tolerance by controlling the interfaces in concentrically layered structures printed with a custom designed mandrel-bed DIW printer and nanocomposite inks. We hypothesized that the damage tolerance of the printed parts could be controlled by tuning the bonding at the interfaces in concentric layer 3D printing.

2 MATERIALS AND METHODS

2.1 Materials

Hydroxyapatite (nHA) powder (rod shape nano particles, approximately 30-40nm diameter and 120nm length) was purchased from MKnano Inc. (Mississauga, Canada). Acrylated epoxidized soybean oil (AESO; a plant-derived 3D printable resin with average molecular weight (MW) 1200), Polyethylene glycol diacrylate (PEGDA; MW 250), and Glycerol 1,3-diglycerolate diacrylate (TGDA;MW 348.35), methacrylic anhydride (MAA), Sodium Hydroxide (NAOH) and the photoinitiator phenylbis (2,4,6-trimethyl benzoyl) phosphine oxide (Irgacure 819) were bought from Sigma Aldrich. 4- (dimethyl amino)pyridine (DMAP) was procured from Alfa Aesar Co. A portion of AESO was functionalized with additional methacrylate groups to develop methacrylated AESO with an adopted protocol from [11], [12]. The nanocomposite inks were developed by slowly dispersing heat treated (at 120° for an hour) nHA particles in the resin blend of AESO/mAESO, PEGDA and TGDA according to the compositions listed in Table 1. Irgacure 819 (1 vol% of total ink) was dissolved into the resin using ultrasonic homogenization.

Table 1. Nanocomposite nomenclatures and compositions reported in vol% .

Material	nHA	AESO	mAESO	PEGDA	TGDA
SP30	30	49	-	21	-
mSP30	30	-	49	21	-
SPT30	30	49	-	18.9	2.1
mSPT30	30	-	49	18.9	2.1

2.2 Nanocomposite characterization

The rheological behaviours of the nanocomposite inks (without photoinitiator) were assessed using a constant stress Rheometer (Bohlin Rheologic, CS, Sweden) with a 40mm diameter cone plate arrangement and gap of 0.150 mm. The viscosity and shear yield strength of inks were measured (n=3) at room temperature with shear rates ranging from 0.01 s-1 to 100 s-1 at 30 second intervals. The measured viscosity and shear stress at each changing shear rate was plotted and the shear yield strength of each ink was measured from the Newtonian part with the y-intercept of the shear stress-strain plot.

2.3 Cure depth characterization for UV curing

Cure depth curve of each UV curable nanocomposite was experimentally measured by adopting the protocol from [13]. In this experiment, a ø10mm hole of 1mm thick polytetrafluoroethylene (PTFE) sheet placed over laboratory glass was filled with ink and exposed to a known doses of UV light (385 nm, at 175 mW/cm2 intensity, BlueWave® QX4® LED Spot-Curing System, Dymax Corp., USA) for different time intervals (n=7). The UV dose was calculated from the UV intensity measured using a radiometer (ACCU CAL 50V, Dymax Corp., USA) at the exposure time interval. The thickness of cured ink was measured after removing uncured material with ethanol and the standard cure depth equation (1) adopted from [14] was used to fit the experimental data.

$$C_d = D_p ln \frac{E_{max}}{E_c} \quad (1)$$

Where C_d is the cure depth in cm, E_{max} is energy dose per area in mJ/cm2, E_c is critical energy dose in mJ/cm2 and D_p represents depth of penetration in cm.

2.4 Isotropic and Anisotropic Microstructure

To evaluate the effect of AESO functionalization on interface bonding, beams of SPT30 and mSPT30 resin mix were cast in layers. 0.1 ml of resin was injected for each layer in the 10mm diameter PTFE mold cavity and cured in UV curing chamber (CureZone MKII, Creative CADWORKS, Canada) for 10 seconds. A four-layer beam was notched with razor and snapped to obtain a surface for analysis.

To analyze the effect of interface bonding on damage tolerance of 3D printed nanocomposites, three concentrically layered microstructures of densely deposited rasters were printed in fourteen concentric layers using the mandrel bed 3D printer (Figure 1a). Crisscross (+/-45°) microstructure was printed by altering 45° helix angle at each layer. The bioinspired concentrically layered lamellar microstructures (Bouligand) were printed with SPT30 nanocomposite only. Bouligand microstructures were printed in two configurations: 1) Bouligand (+) - Helix angle increased by 15° at each increasing layer staring from 0° till ~90°, and 2) Bouligand (-) Helix angle decreased by 15° at each increasing layer staring from ~90° till 0°.

Nanocomposite inks were extruded through 0.25” long and 20 ga (ø 0.6mm) general purpose dispensing tips from EFD, Nordson, USA driven by pressurized air. Nanocomposites beams (50 x 5 x 10 mm, L x T x W) were cast in PTFE mold (Figure 1b) as isotropic controls.

2.5 Testing

Beams were cut longitudinally (along the print length) from all printed microstructures (Figure 1c). All cut and cast beams were sequentially polished with 6 µm, 0.05 µm and 0.01 µm sized polycrystalline diamond suspensions (MetaDi supreme Buehler, IL USA) to prepare Single Edge Notch Bending (SENB) beam as per ASTM-E1820 (Figure 1d) for fracture toughness testing. A controlled micro notch was developed in the SENB beams using a sharp razor and fixture shown in Figure 1e. Fracture tests were performed on specimens using a Psylotech µTS (Psylotech Inc.,

USA) mechanical test frame (Figure 1f). Fracture resistance (K_{Ic}) of isotropic and anisotropic microstructures was calculated from the load-deflection test data to determine the effects of microstructural anisotropy.

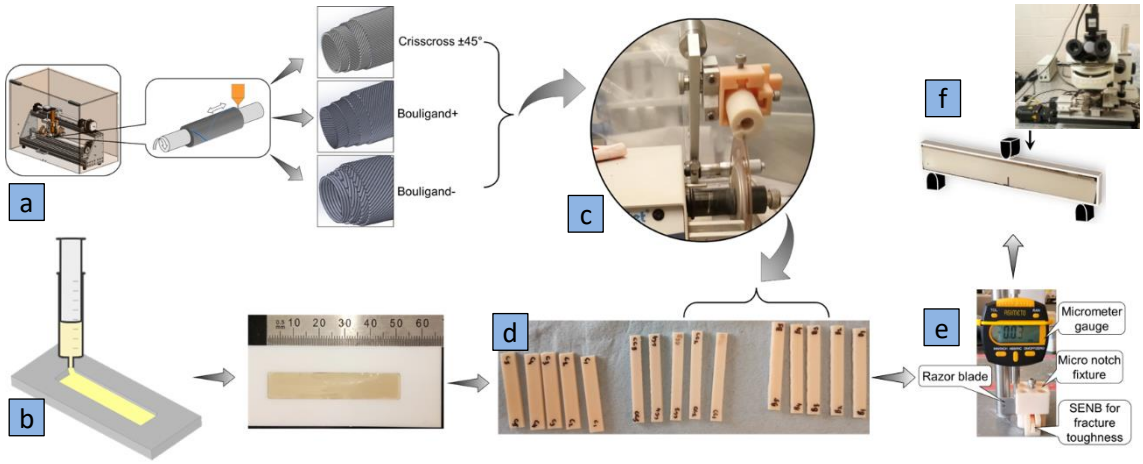

Figure 1. a) Mandrel bed printer and printed microstructures. b) Cast beams as isotropic microstructure controls. c) SENB beams cut from printed microstructures. d) Polished isotropic and anisotropic SENB beams. e) Micro notch developed in the SENB beams. f) SENB tested for fracture toughness under three-point bending

2.6 Microscopic Inspection of Interfaces

Printed microstructures were cut transversely and sequentially polished with diamond suspension to analyze the interfaces developed in the printed microstructures. The polished surface of each printed microstructure was imaged using a Quanta FEG 250 (ThermoFisher Scientific, USA) scanning electron microscope (SEM) at 50x and 100x magnification and 20kV voltage in low vacuum mode. The snapped surfaces of cast resin and fractured surfaces of SENB specimens were also analyzed using SEM to examine the interfaces.

3 RESULTS AND DISCUSSION

3.1 Rheology and Cure Depth

All nanocomposite ink exhibited pseudo plastic behaviour with shear thinning with changing shear rate. The viscosity and shear yield strength of each nanocomposite was determined and listed in Table 2. The rheological behaviour of the nanocomposites was evaluated to understand their suitability for 3D printing. Shear yield strength is an important property which characterizes the ink's ability to hold the extruded profile. Shear yield strength is critical in mandrel bed DIW due to the dynamics associated with rotating bed. All nanocomposites tested had some degree of shape holding, which was lower than the recommended 50 Pa shear yield strength for DIW [10]. Interaction between phases (nHA particles and resin matrix) resulting from non-covalent hydrogen bonding and uniform dispersion of nHA particles contributes to the shear yield strength. SPT30 and mSPT30 nanocomposites containing TGDA had greater shear yield strength than the SP30 and mSP30 nanocomposites.

Table 2.Data are presented as mean ± SD (n = 3)

Material	Viscosity (Pa.s.)	Shear yield (Pa)	Depth of penetration (µm)
SP30	368.2 ±19.9	17.0 ±0.8	216.6 ±4

SPT30	223.1 ±6.8	24.7 ±1.3	170.3 ±4
mSP30	265.6 ±2.1	17.2 ± 0.3	221.1 ±8
mSPT30	302.7 ±4.7	40.1 ± 1.0	226.6 ±6

The UV initiated free radical polymerization crosslinked the functional acrylate and methacrylate groups in the resin mix to cure the nanocomposite. The desired UV dose and curing efficiency of nanocomposite was evaluated with the depth of UV penetration. The mAESO nanocomposites had greater depth of penetration compared to AESO.
SPT30 and mSPT30 resin beams were cast in layers with fixed volume of resin per layer. SEM images of resin beams had shown wider interfaces between the cast layers in SPT30 cast resin than mSPT30 cast resin (Figure 2a-d). The functionalized groups in mSPT resin possibly have enhanced the crosslinking and compacted the size of interface in mSPT resin. Due to wider interface of SPT resin in cast layers (Figure 2b), SPT30 nanocomposite was selected to print bioinspired microstructures to evaluate the contribution of interfaces to fracture toughness.

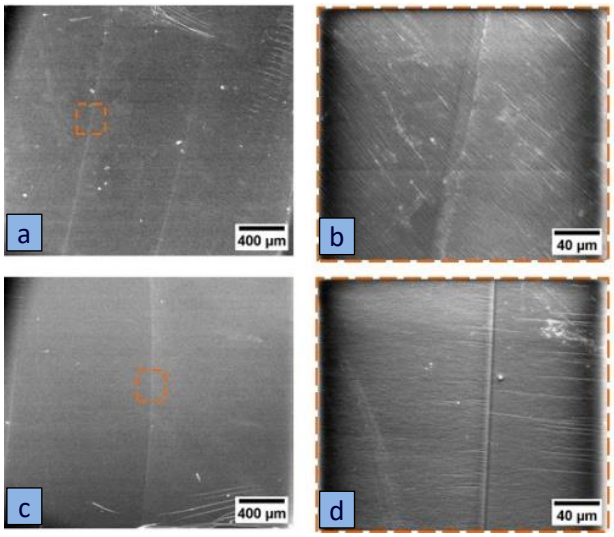

Figure 2. Interfaces in cast resins (n=3), a) SPT30 only resin cast layers. b) Inset view of interface from image a. c) mSPT30 only resin cast layers. d) Inset view of interface from image c.

3.2 Fracture Toughness Results

All Crisscross microstructures of nanocomposites have shown reduction in fracture toughness. The defects resulting from DIW could potentially have reduced the fracture toughness of printed microstructures compared to respective isotropic controls (Figure 3a). Both isotropic and anisotropic microstructures of mSP30 and mSPT30 nanocomposite have shown higher fracture resistance compared to SP30 and SPT30 microstructures, which possibly resulted from higher strength due to higher crosslinking (Figure 3a). However, the load-deflection curves of isotropic and anisotropic microstructures of SP30 and SPT30 demonstrated stable tearing behaviour (Figure 3c,d). The load-deflection curves of mSP30 and mSPT30 isotropic microstructure displayed brittle failure with unstable crack growth (Figure 3c,d). Unlike mSP30, the mSPT30 anisotropic microstructure load deflection curve displayed relatively stable crack growth with multiple pop-ins (Figure 3d). The pop-in resulted from breaking of raster and opening of interfaces at each layer and deflection of crack between layers.
To analyze the contribution of microstructural interfaces on damage tolerance of printed parts, fracture resistance of Bouligand microstructures printed with SPT30 was evaluated. No significant difference was observed between SPT30 isotropic and Bouligand (+) microstructure. SPT30 the Bouligand(-) microstructure had the highest fracture

toughness among all nanocomposites and all printed microstructures. Bouligand(-) microstructure has shown 15% and 8% greater fracture toughness compared to SPT30 and mSPT30 isotropic microstructures respectively. The perpendicular alignment of the rasters ahead of the crack tip in the Bouligand(-) microstructure blunted the crack tip and increased the fracture toughness.

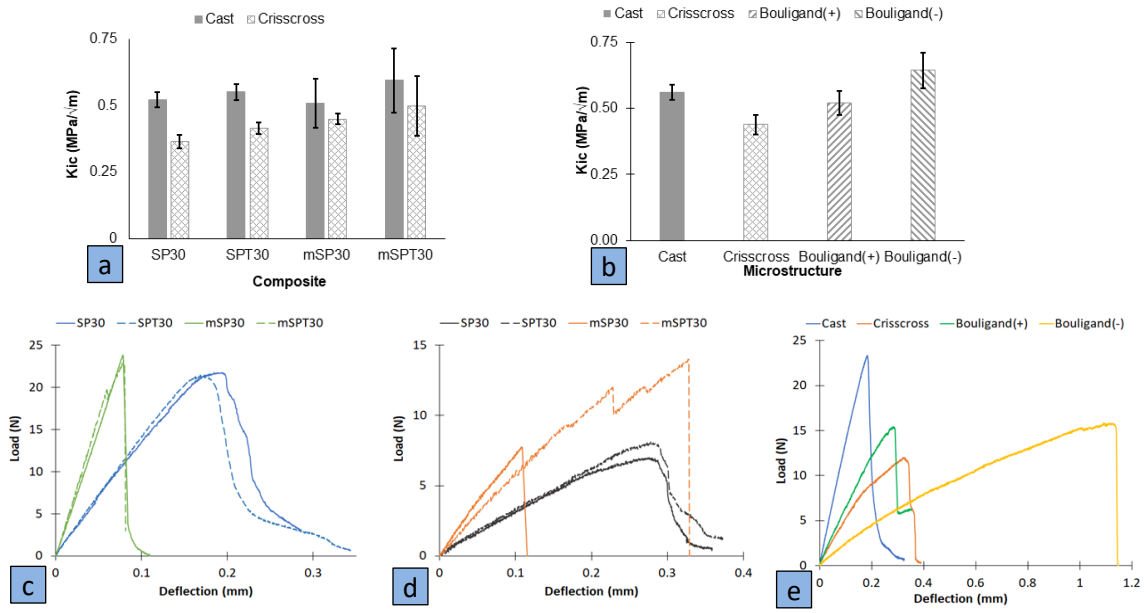

Figure 3. Fracture toughness test results, a) Fracture resistance comparison between isotropic and anisotropic microstructures of nanocomposites. b) Effect of microstructure variation on fracture resistance of SPT30. c) Representative Load vs Deflection curves of isotropic microstructure of nanocomposites. d) Representative Load vs Deflection curves of anisotropic microstructure of nanocomposites. e) Representative Load vs Deflection curves of various microstructure of SPT30 nanocomposite. Data are presented as mean ± SD (n = 5 specimens of each microstructure)

3.3 Microscopy Inspection

3.3.1 Microstructural Interfaces

The SEM analysis of the transverse cross-section of SPT30 printed microstructures revealed distinctly oriented rasters through the noticeable microstructural interfaces (Figure 4a-i). Distorted interfaces were observed in the printed SPT30 microstructures. The fractured surfaces of printed microstructures were studied with SEM to correlate the contribution of interfaces with fracture toughness of printed microstructures. The fractured surfaces of SP30 and SPT30 printed microstructures (Figure 5a, d-f) revealed rough and wavy surfaces due to the stable tearing. Contrarily the brittle fracture of mSP30 printed microstructures revealed clean fracture surfaces (Figure 5b). The fractured surface of mSPT30 nanocomposite (Figure 5c) showed irregular and wedge morphology indicating crack deflection between layers and rasters. mSPT30 fractured surface exhibited clean fractures surfaces of raster indicating brittle failure at raster. Uniform and round morphology of rasters (Figure 5c) observed at fractured surfaces of mSPT30 microstructure, which resulted from the high shear yield strength (40 Pa) of the nanocomposite (Table 2). Fractured surfaces of STP30 microstructures revealed rough surface and opening of microstructural interfaces at bonded layers (Figure 5d-f). Opening of surfaces during fracture dissipates mechanical energy inhibiting stress concentration and restricting crack growth [15].

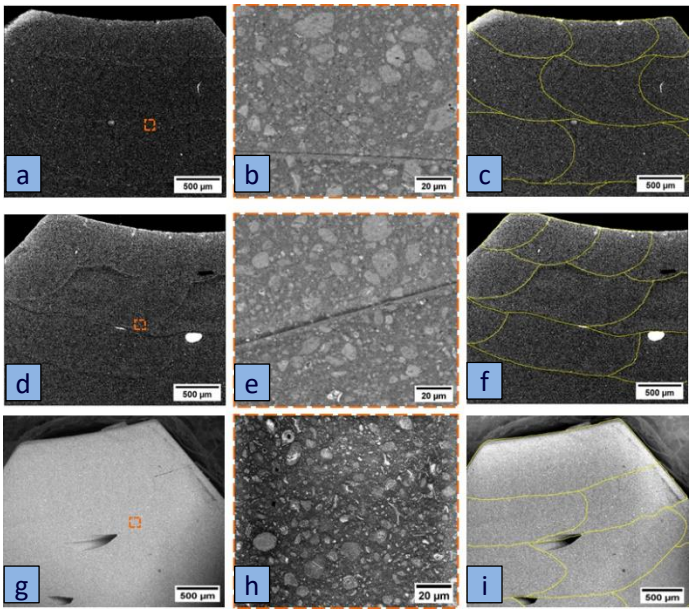

Figure 4. Interfaces in microstructures (n=3), a) SPT30 Crisscross microstructure. b) Inset view of interface from image b. c) Traced interfaces from image a. d) SPT30 Bouligand(+) microstructure. e) Inset view of interface from image d. f) Traced interfaces from image d. g) SPT30 Bouligand(-) microstructure. h) Inset view of interface from image g. i) Traced interfaces from image g.

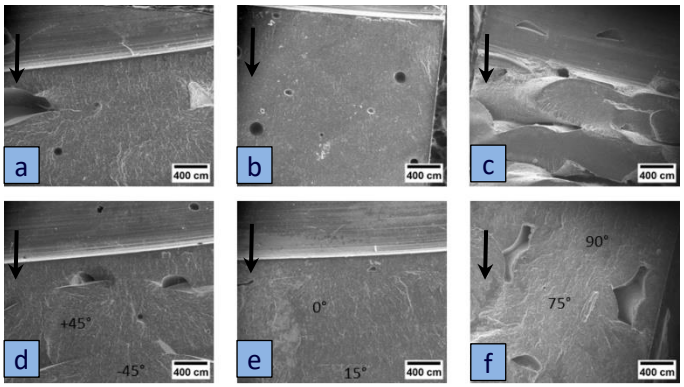

Figure 5. Fractured surfaces of microstructures (n=3), a) SP30 Crisscross. b) mSP30 Crisscross. c) mSPT30 Crisscross. d) SPT30 Crisscross. e) SPT30 Bouligand(+). f) SPT30 Bouligand(-). Arrow indicating direction of crack growth

3.4 Conclusion

Mandrel bed printing enabled us to print bioinspired microstructures and tune the bonding at the interfaces in the printed microstructures. The interfaces in photocurable DIW printed structures made significant contributions to regulating damage tolerance of the printed structure. This study demonstrated that interfaces in photocurable nanocomposites were more effective in enhancing damage tolerance of 3D printed nanocomposite structures than functionalization of the matrix. SPT30 ink reported lower shear yield strength. The SPT30 nanocomposite which was used to evaluate contribution of interface bonding on damage tolerance didn't have adequate shape holding to

retain the shape of extruded raster. A lower shear yield strength could potentially have contributed to inadequate shape holding of the ink.

4 REFERENCES

[1] B. Derisi, S. V. Hoa, D. Xu, M. Hojjati, and R. Fews, "Mechanical behavior of carbon/PEKK thermoplastic composite tube under bending load," *J. Thermoplast. Compos. Mater.*, vol. 24, no. 1, pp. 29–49, 2011, doi: 10.1177/0892705710367978.

[2] H. Yazdani Sarvestani, "Effects of layup sequences on stresses of thick composite cantilever tubes," *Adv. Compos. Mater.*, vol. 26, no. 3, pp. 273–294, 2017, doi: 10.1080/09243046.2015.1111795.

[3] B. Ji and H. Gao, "Mechanical properties of nanostructure of biological materials," *J. Mech. Phys. Solids*, vol. 52, no. 9, pp. 1963–1990, 2004, doi: 10.1016/j.jmps.2004.03.006.

[4] P. Fratzl and R. Weinkamer, "Nature's hierarchical materials," *Prog. Mater. Sci.*, vol. 52, no. 8, pp. 1263–1334, 2007, doi: 10.1016/j.pmatsci.2007.06.001.

[5] Z. Liu, Z. Zhang, and R. O. Ritchie, "Structural Orientation and Anisotropy in Biological Materials: Functional Designs and Mechanics," *Adv. Funct. Mater.*, vol. 30, no. 10, p. 1908121, Mar. 2020, doi: 10.1002/adfm.201908121.

[6] A. J. Crosby and J. Y. Lee, "Polymer nanocomposites: The 'nano' effect on mechanical properties," *Polym. Rev.*, vol. 47, no. 2, pp. 217–229, 2007, doi: 10.1080/15583720701271278.

[7] H. Gojzewski *et al.*, "Layer-by-Layer Printing of Photopolymers in 3D: How Weak is the Interface?," *ACS Appl. Mater. Interfaces*, vol. 12, no. 7, pp. 8908–8914, 2020, doi: 10.1021/acsami.9b22272.

[8] V. Saygin, K. Snapp, A. E. Gongora, R. Kolaghassi, and K. A. Brown, "Mechanical Consequences of Oxygen Inhibition in Vat Polymerization," *Adv. Mater. Technol.*, vol. 8, no. 12, pp. 1–8, 2023, doi: 10.1002/admt.202202022.

[9] A. R. Studart, "Additive manufacturing of biologically-inspired materials," *Chem. Soc. Rev.*, vol. 45, no. 2, pp. 359–376, 2016, doi: 10.1039/c5cs00836k.

[10] D. Mondal, A. Srinivasan, P. Comeau, Y. Toh, and T. L. Willett, "Acrylated epoxidized soybean oil / hydroxyapatite-based nanocomposite scaffolds prepared by additive manufacturing for bone tissue engineering," *Mater. Sci. Eng. C*, vol. 118, no. May 2020, p. 111400, 2021, doi: 10.1016/j.msec.2020.111400.

[11] A. Schwab, R. Levato, M. D'Este, S. Piluso, D. Eglin, and J. Malda, "Printability and Shape Fidelity of Bioinks in 3D Bioprinting," *Chem. Rev.*, vol. 120, no. 19, pp. 11028–11055, 2020, doi: 10.1021/acs.chemrev.0c00084.

[12] W. Liu, T. Xie, and R. Qiu, "Biobased Thermosets Prepared from Rigid Isosorbide and Flexible Soybean Oil Derivatives," *ACS Sustain. Chem. Eng.*, vol. 5, no. 1, pp. 774–783, 2017, doi: 10.1021/acssuschemeng.6b02117.

[13] P. Comeau and T. Willett, "Printability of Methacrylated Gelatin upon Inclusion of a Chloride Salt and Hydroxyapatite Nano-Particles," *Macromol. Mater. Eng.*, vol. 304, no. 8, pp. 1–12, 2019, doi: 10.1002/mame.201900142.

[14] J. H. Lee, R. K. Prud'homme, and I. a. Aksay, "Cure depth in photopolymerization: Experiments and theory," *J. Mater. Res.*, vol. 16, no. 12, pp. 3536–3544, 2001, doi: 10.1557/JMR.2001.0485.

[15] A. TL, *Fracture Mechanics : Fundamentals and Applications*, 2nd ed. CRC Press, 1995.